Thermophysical modeling of raw glaze liquidus temperature and viscosity*

Peter Y. Hsieh†

National Energy Technology Laboratory
Research & Innovation Center
Materials Engineering & Manufacturing Directorate
1450 Queen Ave SW
Albany, OR 97321-2198, USA

Phone: 1-541-918-4501
Fax: 1-541-967-5845
E-mail: pyhsieh@alum.mit.edu

Intended for submission to
International Journal of Applied Glass Science

Date of this version: December 22, 2021

---

† Corresponding author (ORCID 0000-0001-9010-4863)

Abstract

Raw glazes, which do not contain pre-melted glass frits, are widely used due to their low cost. The natural variability of the mineral compositions used in raw glazes affects their viscosity during firing. Molten glaze viscosity plays an important role in determining the final surface quality; therefore, it is important to determine how raw glaze composition and firing conditions affect viscosity. Thermophysical modeling provides a way to evaluate the liquidus temperature and viscosity of molten glazes as a function of composition and oxygen activity. Equilibrium phase volume fraction and composition of 242 raw glaze recipes were evaluated under oxidizing and reducing conditions. Undissolved or precipitation of solid phases explain the secondary flux transition from anti-fluxing to fluxing near the liquidus temperature. The liquidus temperature and viscosity of iron glazes decrease as a function of increasing iron content under a reducing atmosphere. The empirical probability distribution of molten glaze viscosity follows a lognormal distribution, with lead glazes having significantly lower viscosity compared with glazes without lead. The peak firing temperature viscosity of lead-free glazes is near the working point of glass. Multiple linear regression analysis shows that the peak firing temperature viscosity and liquidus temperature significantly predict the viscosity factor.

Keywords

CALPHAD, glaze, Modified Quasichemical Model, multiphase flow, viscosity factor

1. Introduction

Glazes satisfy both functional and aesthetic needs in ceramics fabrication. In addition to sealing porosity and waterproofing the ceramic body, glazes also add color and a glossy or matt surface finish. Molten glaze viscosity is an important factor in surface quality. Pinholes may form if the viscosity is too high; conversely, the glaze may run freely if the viscosity is too low [1]. Estimates of molten glaze viscosity are as low as 0.7 to 2 Pa·s [2] and as high as10^3 to 10^4 Pa·s [3]. The former is comparable to the room temperature viscosity of glycerin, while the latter corresponds to the working point and flow point of glass, respectively. The lack of agreement between these estimates means there is no effective guidance for optimal molten glaze viscosity, particularly the maturation of raw glazes.

During maturation, the constituent minerals in a raw glaze melt to form a vitreous coating and fuse to the ceramic body at the same time. While they are less costly to produce than glazes that incorporate pre-melted glass frits, the melting behavior of raw glazes is less predictable. This is partly due to the natural variability of mineral composition from different mines or quarries. Moreover, the heating schedule can also affect the maturation of raw glazes. Understanding how these variables affect molten raw glaze viscosity is essential for good results with raw glazes.

Molten glaze viscosity measurements have largely been limited to fritted glazes [4-8]. In comparison, few experimental methods have been applied to measure molten raw glaze viscosity. Beam [9] studied the compositional variability in molten feldspathic glaze viscosity by measuring the diameter of fused cones. Additionally, fixed point measurements via hot stage microscopy [10] has been used to study raw glazes [11, 12]. Neither approach measures the dynamic or absolute viscosity of the molten glaze. As a result, raw glaze recipes are developed

and adjusted principally through time consuming trial-and-error testing in the studio or at the fabrication facility.

Computational modeling offers a new approach to studying molten raw glaze viscosity that can rapidly explore the effect of composition, temperature, and oxygen activity. The calculation of phase diagrams (CALPHAD) method [13] uses thermochemical databases and Gibbs energy minimization software to predict equilibrium phases present as a function of oxide composition and temperature. The liquidus temperature of multicomponent oxide melts is determined readily through CALPHAD. Once the molten phase composition and liquidus temperature have been determined, a suitable viscosity model can be used to estimate the molten glaze viscosity. The Modified Quasichemical Model (MQM) [14] is a promising candidate, as it is based on the molten phase structure, specifically the molar fraction of free, bridging, and non-bridging oxygen atoms present. It has been used previously to study the viscous deformation of pyrometric cones [15] and fusibility of coal ash [16]. Lastly, the Einstein-Roscoe equation [17] is used to calculate the effective viscosity of subliquidus melts as a function of the intrinsic viscosity and solid volume fraction. The equilibrium viscosity of fully molten and partly molten raw glazes can thus be estimated readily as a function of composition, temperature, and oxygen activity.

2. Modeling

The oxide composition of molten raw glaze [1, 9, 11, 18-21], fritted glaze [4, 22], glass [10, 23-25], and molten magma [26, 27] were analyzed using a commercial CALPHAD program (FactSage, version 8.1, Equilib Module, FTOxid and FactPS databases) to estimate their liquidus temperature (T_{liq}) as well as their phase fraction and composition at the peak firing temperatures. Compositions given as oxide mass fraction in the source were used as published; otherwise,

Table 1 was used to convert mineral mass fraction to oxide mass fraction. The arithmetic mean of the highest and lowest peak firing temperatures when a firing range is specified (e.g. 1230 °C for cone 5 to 8 or 1200 to 1260 °C) are used where a temperature range is specified. Oxygen activity was evaluated from oxidizing ($aO_2 = 0.21$), weakly reducing ($aO_2 = 10^{-3}$), and strongly reducing ($aO_2 = 10^{-5}$) conditions down to $aO_2 = 10^{-6}$, at 1 atm. The system is assumed to be at equilibrium, associated with long firing times and high peak temperatures, with no metastable phases present in the model output.

The effect of silicate liquid immiscibility in the K_2O-FeO-Al_2O_3-SiO_2 system [28] on viscosity was studied using the FTOxid-SLAGA phase single-phase or possible two-phase immiscibility options. The molten silicate phase with the larger volume fraction is assumed to be the continuous phase. The contribution of the dispersed phase to the effective viscosity is estimated via equation 1 [29]:

$$\eta_r \left[\frac{2\eta_r + 5K}{2 + 5K}\right]^{3/2} = \left(1 - \frac{\phi}{\phi_m}\right)^{-2.5\phi_m} \quad (1)$$

where η_r is the relative viscosity (ratio of emulsion viscosity to continuous-phase viscosity), ϕ is the volume fraction of the dispersed phase, and K is the viscosity ratio (η_d / η_c or ratio of dispersed phase viscosity to continuous-phase viscosity).

The solid volume fraction (Φ) is calculated by first estimating the volume of each solid and molten phase present, and then dividing the sum of the solid volume by the total volume. Solid phase volume is based on mass and the density of the mineral or pure chemical compound at ambient pressure and temperatures as shown in Table 2. The primary contribution to changes in solid phase density is expected to be phase transformations. For example, tridymite density is approximately 14% lower than quartz density at ambient temperature and pressure [30]. The decrease in solid phase density due to thermal expansion is assumed to be negligible in

comparison, as demonstrated by the decrease in plagioclase feldspars density by less than 2% when heated from ambient temperature to over 900 °C [31]. Molten phase density was calculated with its composition from the output data, based on partial molar volumes of oxides present [32-36], and used to calculate the molten phase volume from its mass.

The intrinsic viscosity (η_0) of the molten phase as a function of composition and temperature was calculated using the Modified Quasichemical Model (FactSage, version 8.1, Viscosity Module, Viscosity Module, Melts database for $T > T_{liq}$ - 200 °C and Glasses database for $T < T_{liq}$ – 200 °C) with up to 14 oxide and 11 fluoride compounds. For molten raw glazes containing stable solid phase or phases, the Einstein-Roscoe equation was used to estimate the effective viscosity (η):

$$\eta = \eta_0 \left(1 - \frac{\Phi}{\Phi_{max}}\right)^{-2.5} \quad (2)$$

where Φ_{max} is the maximum packing fraction of the solid phase (i.e. the critical solid phase volume fraction). Jamming transition simulations[37, 38] and rheological measurements of spherical particle suspensions[39] suggest that Φ_{max} is around 0.64. For this study, a value of 0.637 [29] was used for Φ_{max} for this study.

3. Results and Discussion

3.1 Effect of oxygen activity on liquidus temperature and secondary flux transition

Raw glazes become fully molten above their liquidus temperatures upon reaching equilibrium. When the peak firing temperature is less than the liquidus temperature, undissolved or newly precipitated solid phases can scatters light, which gives the resultant glaze a matt or opaque finish. Figure 1 plots the liquidus and peak firing temperatures of 175 lead-free glazes [1, 40] and 12 lead glazes [18, 19] with matt and gloss (i.e. transparent, semitransparent, or bright) finishes (see A. The liquidus temperature calculation accounts for the possibility of two-phase

Table 1 Average oxide and fluorine mass fraction of common raw glaze minerals and metallic compounds. Zinc oxide (100 % ZnO) and trace P_2O_5 (< 0.08 %) and SO_3 (< 0.04 %) in ball clay, china clay, and Cornish stone were also incorporated into the model.

	SiO_2	**Al_2O_3**	**CaO**	**MgO**	**MnO**	**Li_2O**	**Na_2O**	**K_2O**	**Fe_2O_3**	**FeO**	**PbO**	**TiO_2**	**F**	**LOI**	**Ref.**
Ball clay	46.8	34.8	0.42	0.2	0	0	0.85	0.31	1.59	0	0	0.21	0	14.8	[41, 42]
Bentonite	57.6	22.2	1.19	2.57	0	0	1.62	0.43	1.81	0	0	0.01	0	12.6	[40, 43]
China clay	44.9	38.7	0.04	0.06	0	0	0.02	0.17	0.60	0.08	0	1.26	0.01	14.1	[44, 45]
Cornish stone	71.9	16.2	1.75	0.03	0	0	3.1	5.33	0.14	0	0	0.09	0.14	1.29	[40, 46, 47]
Dolomite	1.5	0.6	31.0	20.1	0.03	0	0.03	0.07	0.26	0	0	0	0	46.5	[40, 48]
Feldspar (potash)	66.6	18.6	0.39	0	0	0	2.89	11.4	0.1	0	0	0	0	0.07	[40, 47]
Feldspar (soda)	67.5	19.4	1.84	0	0	0	7.2	3.65	0.06	0	0	0	0	0.41	[40, 47]
Flint	99.9	0.2	0	0	0	0	0	0	0	0	0	0	0	0	[40, 49]
Lepidolite	49.2	26.7	0.05	0.01	0.18	4.25	1.3	10.4	0.28	0.11	0	0	5.82	1.7	[50]
Lithium carbonate	0	0	0	0	0	40.4	0	0	0	0	0	0	0	59.6	[1]
Nepheline syenite	59.0	23.8	0.55	0	0	0	9.2	7.14	0.10	0	0	0	0	0.1	[40, 47]
Red clay	57.5	14.6	5.76	2.67	0	0	0.8	3.24	5.19	0	0	0.80	0	9.43	[51]
Red iron oxide	0	0	0	0	0	0	0	0	100	0	0	0	0	0	[1]
Spodumene	65.0	27.0	0	0	0	8.0	0	0	0	0	0	0	0	0	[40]
Talc	55.2	1.1	2.28	30.9	0	0	0	0	1.65	0	0	0	0	8.9	[40, 52]
White lead	0	0	0	0	0	0	0	0	0	0	86.3	0	0	13.7	[53]
Whiting	0.23	0	55.4	0.05	0.13	0	0	0	0.05	0	0	0	0	44.1	[40, 45]
Wollastonite	51.4	0.8	45.2	0.98	0.05	0	0.05	0	0.48	0	0	0.02	0	0.98	[40, 54]

Table 2 Ambient density of stable solid minerals and chemical compounds.

FactSage phase	Mineral or compound	ρ (g/cm³)	Ref.
a'(Ca,Sr,Ba)2SiO4	calcium orthosilicate	3.27	[55]
CaSiO3_Ps-wollastonite	pseudowollastonite	2.90	[56]
Clinopyroxene#1 and #2	clinopyroxene	3.19	[57]
Cordierite	cordierite	2.63	[58]
Feldspar#1	feldspar	2.65	[52]
Leucite	leucite	2.5	[58]
M2O3(Corundum)#1	corundum-hematite	4.62	[59]
Melilite	melilite	3.0	[58]
Mg4Al10Si2O23_Sapphirine	sapphirine	2.63	[60]
Mullite#1	mullite	3.16	[30, 61]
Olivine#1	olivine	3.74	[62]
SiO2_Tridymite(h)	tridymite	2.28	[30]
Spinel#1	spinel-hercynite	3.72	[58]
Titania_Spinel	ulvöspinel-geikielite	4.48	[59, 63]
Willemite	willemite	4.10	[64]
Wollastonite	wollastonite	2.98	[52]

immiscibility in the molten glaze. Glazes containing lead melt fully at a significantly lower temperature compared with those that do not contain lead ($F(1,185) = 90.5$, $p < 0.001$). In addition, the average liquidus temperature of matt glazes is significantly lower relative to gloss glazes ($F(1,207) = 38.6$, $p < 0.001$) and is 22 °C higher than the peak firing temperature. In comparison, the average liquidus temperature of gloss glazes is 59 °C lower than their peak firing temperature. In other words, transparent or gloss glazes are far more likely to be fully molten at their peak firing temperature compared with matt glazes. While devitrification of a fully molten glaze can also give rise to a matt finish, transparent glazes cannot have any light scattering solid particles upon reaching the peak firing temperature. Consequently, the liquidus temperature is an important parameter in predicting glaze surface finishes.

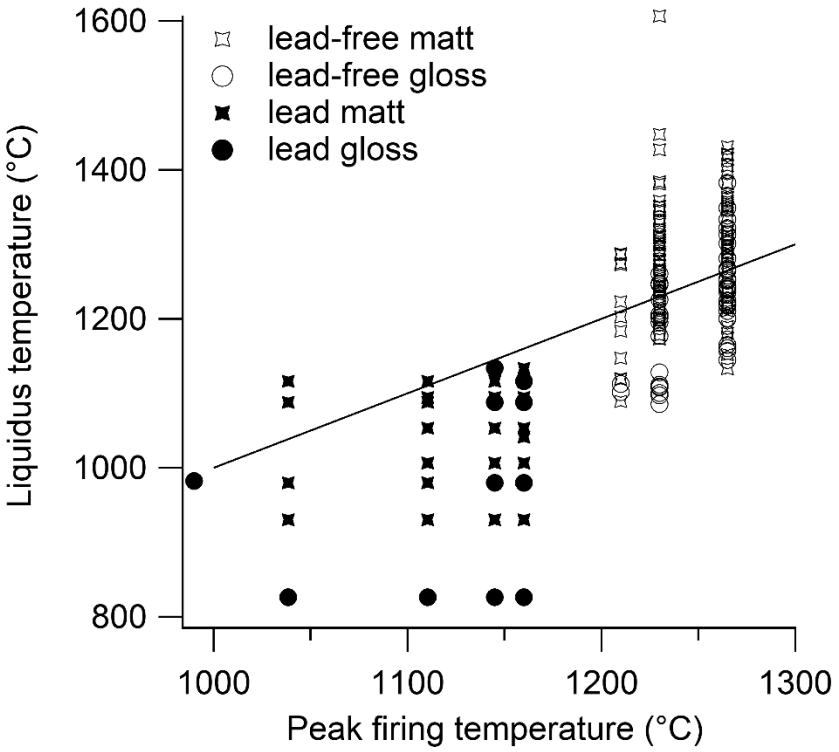

Figure 1 Comparison between the liquidus temperature and peak firing temperature of raw glazes in an oxidizing atmosphere. A line showing 1:1 correlation is plotted for comparison.

The primary phase field describes the crystalline phase that forms first upon cooling a melt below its liquidus temperature. It is thermodynamically stable and is the last to melt if it is present in the glaze recipe. For example, tridymite and cristobalite (high temperature polymorphs of SiO_2) will not dissolve fully until the liquidus temperature is reached. This also applies to recipes that contain wollastonite ($CaSiO_3$) and pseudowollastonite.

Glazes that contain iron oxide become fully molten at progressively lower temperatures when fired under a reducing atmosphere as the oxygen activity is decreased. This is due the reduction of iron(III) oxide (Fe_2O_3) to iron(II) oxide (FeO). Iron oxides are known to be secondary fluxes and have an anti-fluxing effect below 1220 °C for Fe_2O_3 and 895 °C for FeO [53]. This is consistent with Figure 2, which shows the decrease in the liquidus temperature as a function of iron fraction and oxygen activity determined through thermophysical modeling.

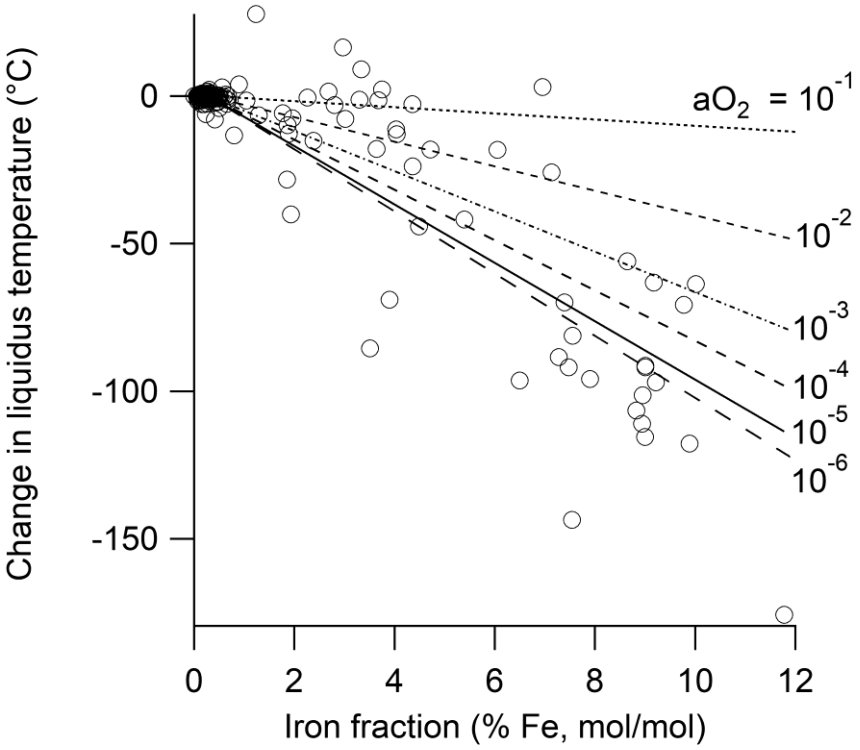

Figure 2 Decrease in liquidus temperature as a function of glaze iron fraction ($aO_2 = 10^{-5}$). Linear regression lines at different oxygen activity are also plotted for comparison. Changes are relative to the liquidus temperature in an oxidizing atmosphere ($aO_2 = 0.21$). See Appendix A for liquidus temperatures in tabular form.

The decrease in the liquidus temperature of iron oxide glazes due to reduction is explained by the transition in the primary phase field from hematite (Fe_2O_3) to magnetite (Fe_3O_4) and sometimes anorthite ($CaAl_2Si_2O_8$), where the majority of iron oxide is present as FeO in the molten phase. The formation of a stable calcium-rich feldspar from potash or soda feldspar occurs as CaO minerals (e.g. whiting, wollastonite, dolomite) through a dissolution-precipitation mechanism mediated by the molten phase. The same mechanism is at work to produce willemite (Zn_2SiO_4) and magnesium-rich olivine (Mg_2SiO_4) from zinc oxide and MgO minerals (e.g. talc and dolomite).

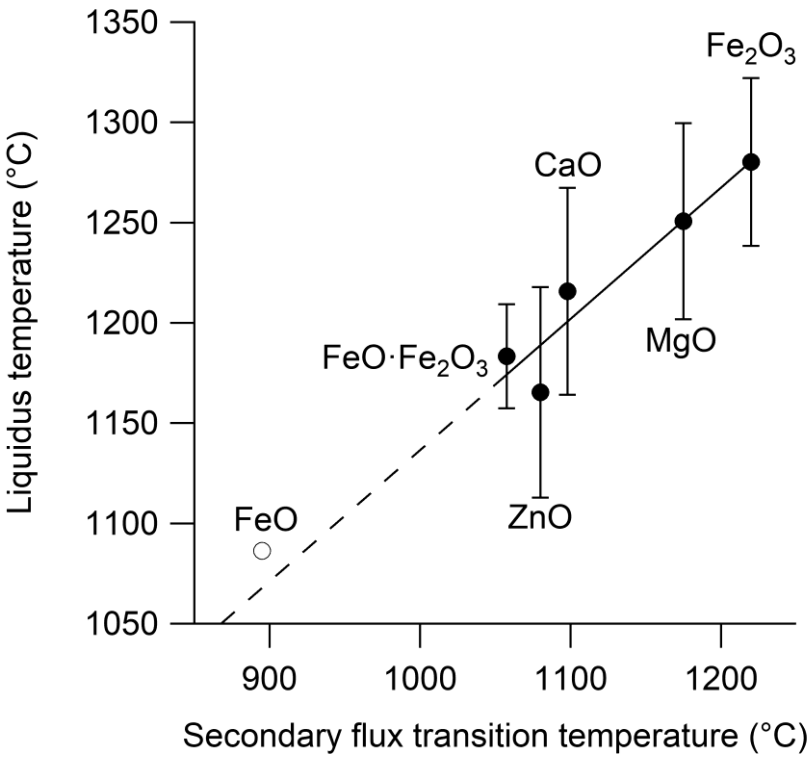

Figure 3 Liquidus and secondary flux transition temperatures [53]. Error bars correspond to one standard deviation. The linear regression line (solid) does not include FeO; the dashed line and open circle for FeO are extrapolated values.

Figure 3 shows the average liquidus temperature of glazes that have primary phase field which clearly corresponds to a single secondary flux: hematite (Fe_2O_3), forsterite (MgO), wollastonite or pseudowollastonite (CaO), and willemite (ZnO). The secondary flux transition temperature of magnetite, a $FeO{\cdot}Fe_2O_3$ spinel, is assumed to be the average of the values for FeO and Fe_2O_3. The liquidus temperature for pure FeO is extrapolated from the average liquidus temperatures of hematite and magnetite. For this reason, it is plotted for comparison but not included in the linear regression analysis. The coefficient of determination ($R^2 = 0.90$) shows that the liquidus temperature and secondary flux transition temperature are strongly correlated. The melting of the secondary flux only begins to have an appreciable effect on viscosity between 60 to 130 °C below the liquidus temperature, since precipitation of the stable phases acts to remove

secondary fluxes from the melt. Barium oxide (BaO) has a secondary flux transition temperature of 1185 °C and is predicted to have a corresponding stable oxide mineral with an average liquidus temperature of 1257 °C in molten raw glazes.

3.2. Comparison between viscosity models and measured values

Modeling molten glaze viscosity as a function of composition, temperature, and oxygen activity is complicated by the presence of iron oxide. For example, neither Fluegel's global statistical model, which is based on multiple regression and the widely known SciGlass database [65], nor Giordano [66] et al. multicomponent chemical model for naturally-occurring silicate melts, account for the contribution of both Fe_2O_3 and FeO. Fluegel treats all iron oxide as Fe_2O_3, while Giordano et al. assume all iron oxide as FeO. Unlike these models, MQM uses both Fe_2O_3 and FeO in calculating viscosity. Also, while the multicomponent chemical model is limited to the SiO_2-Al_2O_3-CaO-MgO-MnO-FeO-Na_2O-K_2O-TiO_2-P_2O_5-F system, MQM also includes ZnO, PbO, Li_2O, and B_2O_3. These are oxides present in many glaze recipes. While MQM also accounts for Ti_2O_3, the trace quantities (< 210 ppm, mol/mol) expected to be present in the molten phase are not expected to have a significant effect on viscosity.

Figure 4 plots the viscosity predicted by the global statistical model, multicomponent chemical model, and MQM against experimentally measured viscosities [10, 23, 25-27] in the valid range of each model. The output of all three models are strongly correlated with measured viscosities ($R > 0.99$); however, more extensive use of the global statistical model in this study is precluded by compositional limits on model applicability.

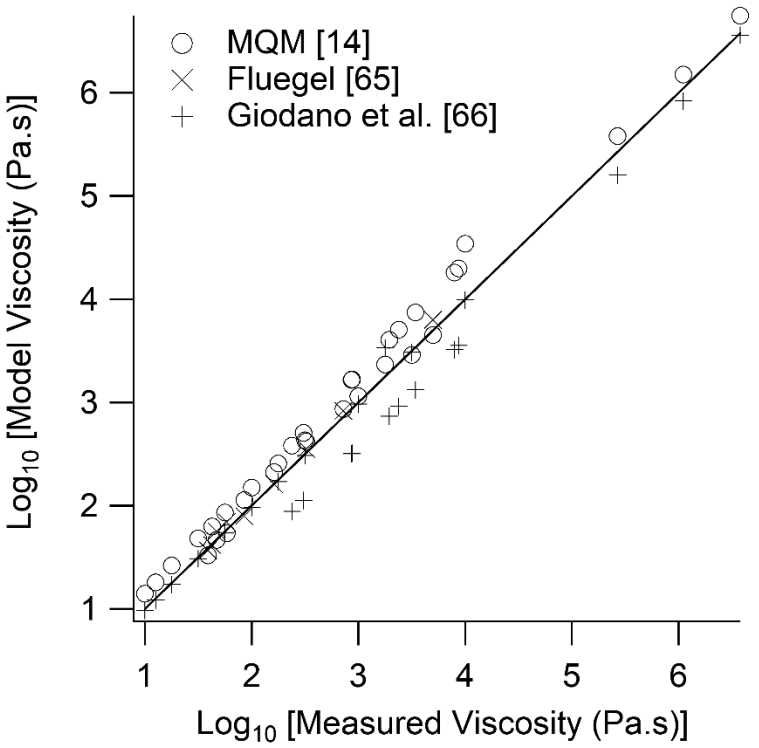

Figure 4 Comparison predicted and measured viscosity from [10, 23, 25] for Fluegel [65] and [26, 27] for Giordano et al. [66]. A solid line showing 1:1 correlation is plotted for comparison.

Table 3 Components of molten frits, glazes, glasses and magmas

Ref.	**SiO_2**	**Al_2O_3**	**CaO**	**MgO**	**ZnO**	**Na_2O**	**K_2O**	**TiO_2**	**B_2O_3**	**Other**
[22]	X	X	X		X	X	X	X	X	CaF_2, NaF, AlF_3
[4]	X	X	X	X	X	X	X		X	PbO
[10]	X	X	X	X		X	X		X	Li_2O
[24]	X	X				X	X			PbO
[25]	X	X	X		X	X	X	X		
[23]	X	X	X	X		X	X		X	Fe_2O_3
[26]	X	X	X	X		X	X	X		MnO, FeO
[27]	X	X	X	X		X		X		MnO, Fe_2O_3

MQM viscosity estimates are compared with dynamic viscosity measured via ball drawn viscometry [22], sinking bar viscometry [10], rotary viscometry [4, 10, 23-27], and fiber elongation [23] for porcelain enamel frits [22], fritted sanitary ware glazes [4], experimental glasses [10], standard reference glasses [24, 25], commercial glasses [23], and magmas [26, 27].

The models and measured viscosity values are plotted in Figure 5. The data is also shown in tabular form in Appendix B. The components of the molten oxides are summarized in Table 3.

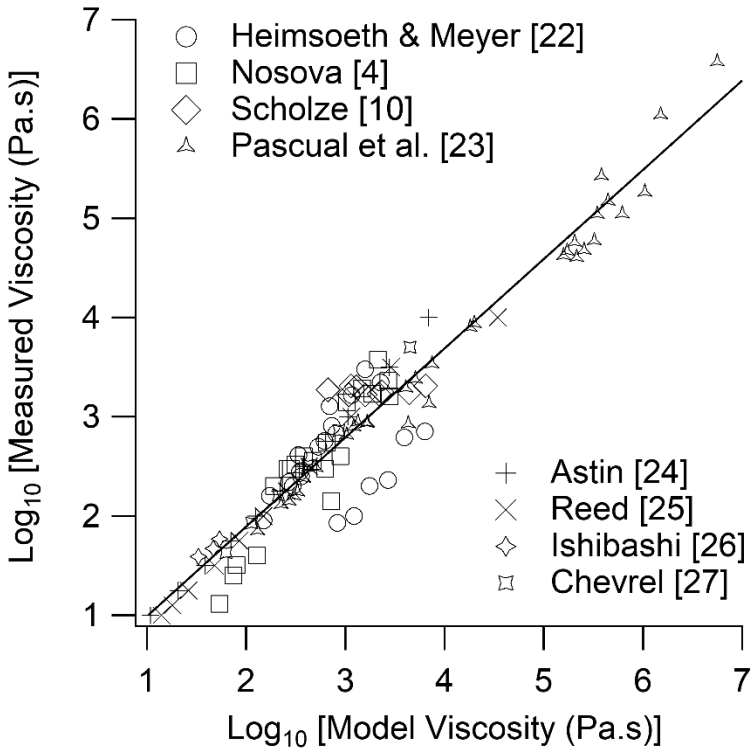

Figure 5 Measured and MQM viscosity of molten frits, fritted glazes, glasses, and magma

Linear regression analysis of the model and measured values show that the two are strongly correlated ($R^2 = 0.93$, $F(1, 112) = 1572$, $p < 0.001$), but the model systematically overestimates the viscosity. The regression line (Equation 3) will be used to correct the model viscosity for molten raw glazes based on the oxide phase composition.

$$log_{10}(\eta_{measured}) = 0.8996\, log_{10}(\eta_{MQM}) + 0.09093 \quad (3)$$

Notably, the model viscosity of lead glass begins to deviate from the measured value above 10^5 Pa·s. For U.S. NIST Standard Reference Material 711 (lead silica glass, 45.32% PbO by mass), this corresponds to 710.4 °C for measured viscosity. All raw glazes studied have a peak

temperature of 970 °C (cone 07) or more, and have lead content ranging from 39 to 51% by mass.

3.3. Effect of silicate liquid immiscibility and oxygen activity on viscosity

The formation of low viscosity Ca-rich (CaO/SiO_2 = 22%, mol/mol) and high viscosity Ca-poor (CaO/SiO_2 = 2%, mol/mol) immiscible molten phases are predicted for around 40% of the raw glazes evaluated in this study. The liquid-liquid emulsion viscosity is 22% lower on average when compared with the corresponding single-phase viscosity. The single-phase and two-phase models are generally in agreement for viscosity values up to 10^4 Pa·s, above which the two models begin to deviate (Figure 6). The lack of agreement occurring in a small number of cases studied (14% of two-phase models and 6 % of the total) is attributable to misidentification of the continuous phase.

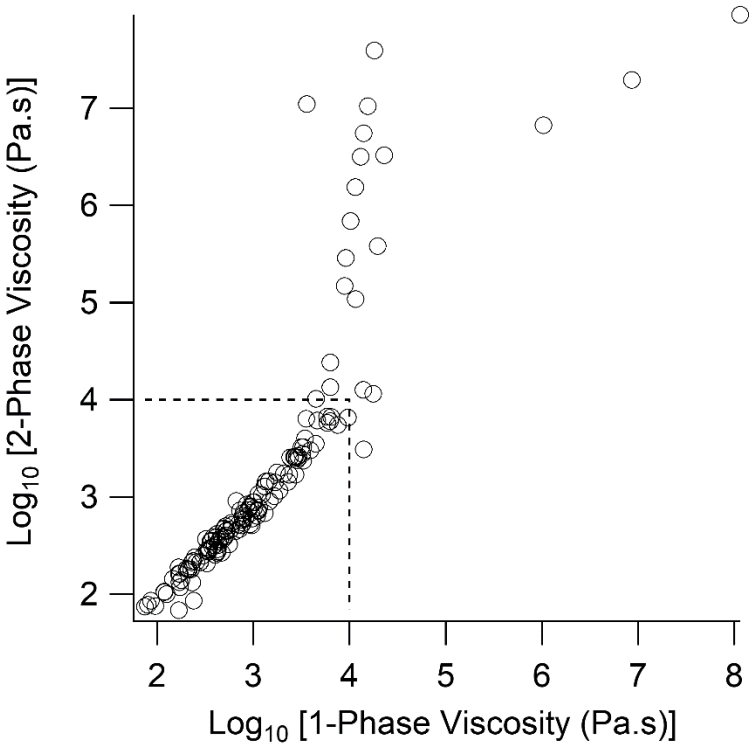

Figure 6 Deviation between single- and two-phase model viscosity above 10^4 Pa·s (dashed line).

Increasing the iron content of a glaze makes it more susceptible to a drop in the effective viscosity under a reducing atmosphere (Figure 7). In addition to the decrease in the liquidus temperature of iron glazes under a reducing atmosphere, the formation of iron(II) oxide decreases the viscosity of a glaze by breaking up bridging Si-O-Si bonds in the molten silicate network. This is consistent with observations of "runny" iron oxide glazes under reduction firing [1] and a warning too much iron oxide can make a glaze too fluid when fired under reducing conditions. In other words, a reducing environment decreases both the solid volume fraction (Φ) and the intrinsic viscosity (η_0) in the Einstein-Roscoe equation, leading to a decrease in the effective viscosity of the molten glaze.

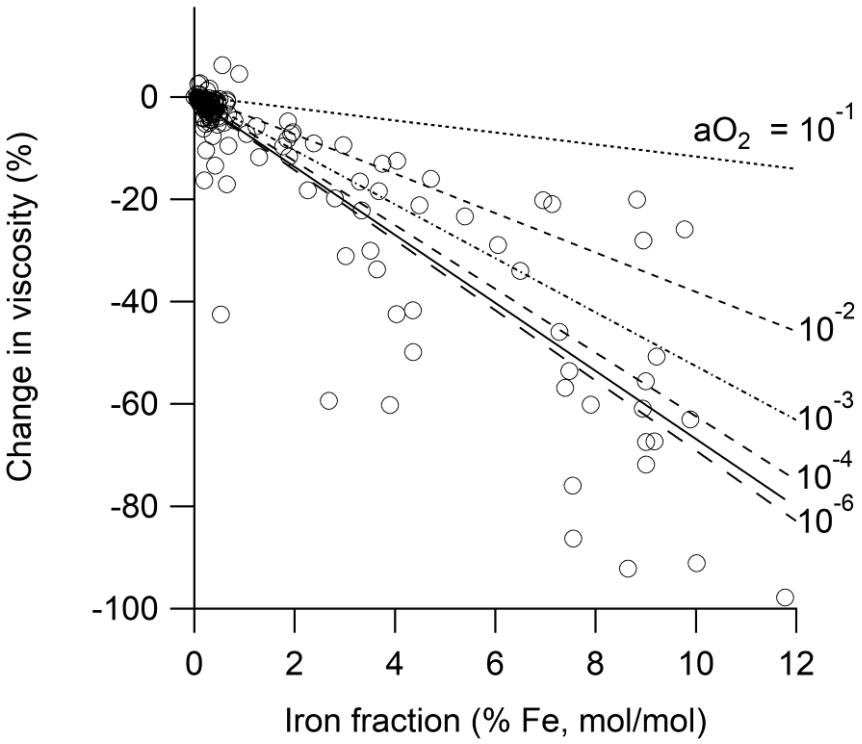

Figure 7 Decrease in the effective viscosity at the peak firing temperature as a function of glaze iron fraction ($aO_2 = 10^{-5}$). Linear regression lines at different oxygen activity are also plotted for comparison. Changes are relative to the liquidus temperature in an oxidizing atmosphere (aO_2 = 0.21). See Appendix A for effective viscosity values in tabular form.

The decrease in the effective viscosity on a glaze containing 12 % (mass/mass) red iron oxide as well as potash feldspar, whiting, ball clay, china clay, and flint (recipe 419 from [1]) is illustrated in Figure 8. The effective viscosity is predicted to be significantly higher under an oxidizing atmosphere compared to reducing atmospheres. The initial drop in the predicted effective viscosity arises from a transition from a high viscosity continuous phase (Ca and Fe-poor) to a low viscosity (Ca and Fe-rich) continuous phase. Since the volumes of the two immiscible molten phases are very close to each other, it is possible that the high viscosity estimate arises from a misidentification of the continuous phase. If this is the case, the effective viscosity may much lower (2.1×10^4 Pa·s). The molten glaze viscosity decreases continually under increasingly reducing conditions as more iron enters the molten phases. The glaze becomes fully molten at the peak firing temperature when oxygen activity is less than 10^{-4}, and the effective viscosity does not decrease significantly thereafter.

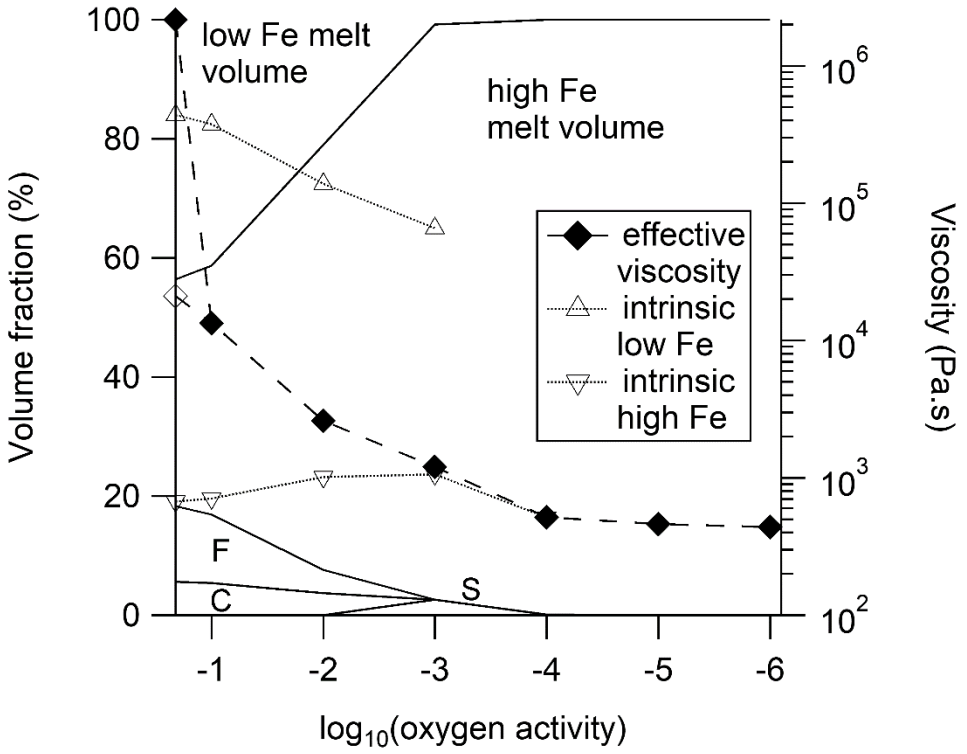

Figure 8 Changes in volume fraction of molten and solid phases: feldspar (anorthite), corundum (hematite), and spinel (magnetite) as well as intrinsic and effective viscosity of a high firing iron stoneware glaze (cone 7 to 9) at 1265 °C as a function of oxygen activity.

3.4. Measurement of molten glaze deformation at constant heat work

Beam [9] measured the diameter of fused cones as a way of quantifying the viscosity of molten feldspathic glazes. The dry powder sample is loaded a conical mold and transferred to an unfired clay disk. After firing, the diameter of the fused raw glaze sample is measured with a caliper. The sample diameter is reported in millimeters is reported as the viscosity factor. Beam noted that the compositions producing good glazes at cone 12 all had similar viscosity factors.

Unlike hot stage microscopy, which measures the temperature at which the sample reaches a predefined geometry under constant rate heating, the Beam viscosity factor measures the extent of deformation under constant heat work. Heat work (i.e., the combined effect of time and temperature) is typically measured with pyrometric cones, which mechanically integrate viscous deformation as a function of time. Viscosity is a function of the pyrometric cone composition and temperature [15]. Consequently, the Beam viscosity factor is not solely a function of viscosity; instead, the time from the onset of deformation to the peak firing temperature must be considered as well.

The onset of deformation at the Littleton softening point ($10^{6.6}$ Pa·s) temperature is strongly correlated with the liquidus temperature in pyrometric cones ($R^2 = 0.83$); consequently, it is useful as a readily calculated proxy variable for the viscous deformation time in raw glaze samples. Table 4 summarizes the liquidus temperature and viscosity of raw glazes containing feldspar, flint, china clay (kaolin), and whiting at cone 12 (1300 °C) under an oxidizing atmosphere. A single molten phase was used for the MQM analysis to avoid misidentification of

the continuous phase as a source of error. Multiple linear regression analysis was used to test whether the liquidus temperature and peak firing temperature viscosity significantly predict the viscosity factor. The result of the regression shows that the two predictors explain 74% of the variance ($F(2,41) = 59$, $p < 0.001$) in the data, and the findings are summarized by equation 4:

$$Viscosity\ Factor = 120.43 - 0.046174\ T_{liq} - 5.0829\ log_{10}(\eta_{1300°C}) \quad (4)$$

Table 4 Liquidus temperature (T_{liq}) and viscosity based on composition of raw glazes [9], identified by member numbers (M#) and corresponding viscosity factors. Good glazes identified in the original work are marked with an asterisk (*).

M#	$T_{liquidus}$ (°C)	$log_{10}(\eta$, Pa·s)		Viscosity factor (mm)	M#	$T_{liquidus}$ (°C)	$log_{10}(\eta$, Pa·s)		Viscosity factor (mm)
		MQM [14]	MCM [66]				MQM [14]	MCM [66]	
1	1461	4.51	5.70	29.5	27	1164	3.15	4.33	48.5
2	1242	4.41	5.51	31.4	28	1204	3.11	4.16	48.3
3	1345	4.34	5.35	36.8	32	1529	3.25	4.77	29.8
4	1280	4.30	5.21	38.5	33	1461	2.84	4.66	35.0
5	1259	4.24	5.04	39.2	34	1387	2.82	4.57	49.0
6	1279	4.19	4.87	39.2	35*	1307	2.81	4.49	49.9
7	1299	4.14	4.73	40.5	36*	1221	2.77	4.30	52.1
8	1318	4.25	4.70	41.0	37	1206	2.74	4.11	53.7
11	1518	4.09	5.46	29.5	38	1205	2.71	3.92	53.6
12	1460	3.83	5.28	32.6	43	1476	2.44	4.41	31.8
13	1398	3.77	5.14	41.8	44	1397	2.43	4.34	42.3
14*	1184	3.72	5.02	43.0	45	1312	2.43	4.27	46.1
15*	1259	3.69	4.88	42.5	46*	1254	2.40	4.08	49.2
16	1192	3.65	4.70	44.7	47	1247	2.37	3.87	53.0
17	1227	3.60	4.54	44.2	48	1241	2.34	3.67	54.1
18	1260	3.56	4.38	43.7	49	1233	2.30	3.47	59.4
21	1560	3.72	5.19	30.2	54	1398	2.24	4.24	36.5
22	1500	3.57	5.03	36.8	55	1307	2.08	4.06	43.3
23	1435	3.28	4.90	45.6	56	1293	2.05	3.83	46.6
24*	1365	3.24	4.80	47.5	57	1289	2.02	3.61	47.9
25*	1290	3.22	4.70	47.0	58	1283	1.99	3.39	50.1
26*	1210	3.18	4.51	48.3	59	1276	1.96	3.18	55.6

The liquidus temperature significantly predict the viscosity factor (β = -0.62, $p < 0.001$), as does the peak firing temperature viscosity (β = -0.51, $p < 0.001$). Figure 9 plots the multiple linear regression results against their corresponding measured viscosity factors. The analysis was repeated using the multicomponent chemical model (MCM), and the multiple regression findings are substantially the same:

$$Viscosity\ Factor = 121.25 - 0.032839\, T_{liq} - 7.6258\, log_{10}(\eta_{1300°C}) \quad (5)$$

where the regression model explains 76 % of the variation ($F(2,41) = 66$, $p < 0.001$). Notably, the MCM effective viscosity is roughly an order of magnitude higher than the values predicted by the MQM model. This is surprising since both models are in agreement when used to calculate the viscosity of molten magmas. The difference may be due to the absence of iron from the raw glaze compositions studied by Beam.

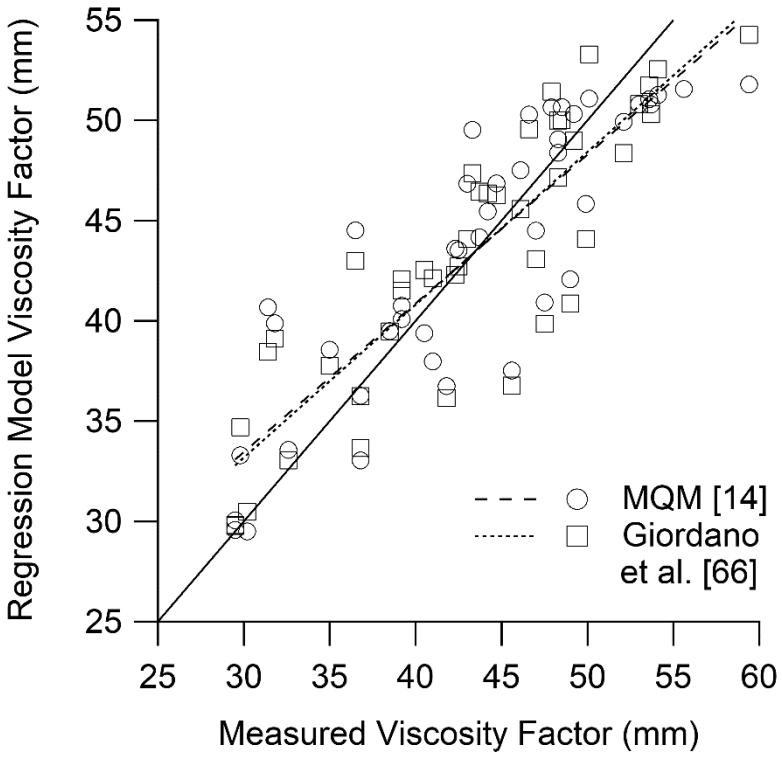

Figure 9 Regression models and measured viscosity factors [9] for feldspathic glazes. A solid line showing 1:1 correlation is plotted for comparison.

3.5. Average viscosity of raw glazes with and without lead

Figure 10 plots the empirical probability distribution of the peak firing temperature viscosity calculated from raw glaze recipes, 14 of which contain lead [18-21] and 201 which do not [1, 9, 11, 40], under oxidizing conditions and using a single-phase molten oxide model. The log-normal distributed viscosity values range from 0.48 to 150 Pa·s for raw glazes with lead and 13 to 7900 Pa·s for raw glazes without lead (Table 5). Glazes with lead are predicted to have significantly lower viscous than glazes without lead ($F(1, 213) = 37.9$, $p < 0.001$), despite the former having peak firing temperatures that are lower (990 to 1160 °C) than the latter (1200 to 1280 °C). This is explained by the lower liquidus temperature of glazes with lead.

A subset (n = 139) of the glaze recipes was analyzed using the multicomponent chemical model. Again, the estimate is roughly an order of magnitude higher than the values predicted by the MQM model.

Table 5 Average peak firing temperature viscosity of glazes with lead and without lead

Glaze	Model	μ	σ	Mean (Pa·s)	Median (Pa·s)	Mode (Pa·s)
with lead	MQM	0.933	0.624	13.4	8.6	3.5
without lead	MQM	2.509	0.693	561	323	107
	MCM	3.353	0.991	5860	2250	333

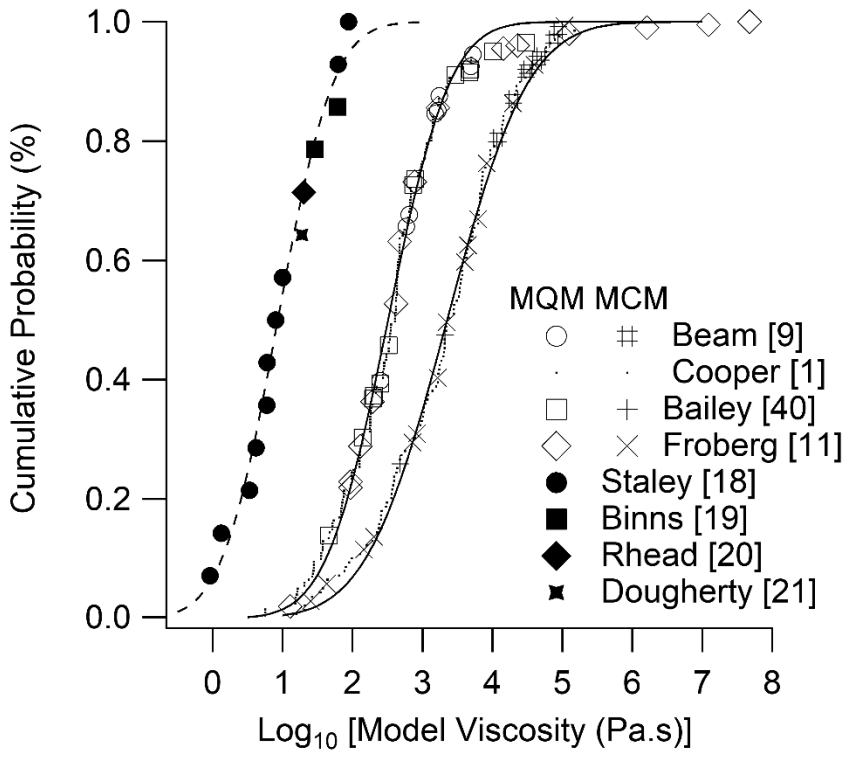

Figure 10 Empirical probability distribution of model raw glaze viscosity with lead (filled symbols) and without lead (open symbols). Dashed (- -) and solid (—) lines show normal distribution models fitted to the lead glaze and lead-free glaze datasets, respectively.

The difference between the peak firing temperature viscosity for raw glazes with lead and those without lead may be explained by Nosova's [4] observation that fritted glazes with lead are less likely to boil up, or form closed or burst bubbles on the glaze surface. Additionally, it is recommended that molten glaze viscosity should be either greater than 600 to 900 Pa·s or less than 40 Pa·s to avoid boiling up. Thermophysical modeling of raw glaze viscosity indicates that the mean viscosity for lead-free glazes at their peak firing temperature is around 600 to 5900 Pa·s, depending on the viscosity model, while the mean viscosity for raw glazes containing lead is 13.4 Pa·s. The former is within the higher viscosity range and the latter is below the lower viscosity limit to avoid boiling up. The lower viscosity limit is in agreement with the 0.7 to 2

Pa·s viscosity range for fast firing tile glazes [2]. In comparison, lead-free glaze viscosity is closer to the flow point of glass (10^3 Pa·s) [3].

4. Conclusions

The liquidus temperature is an important variable for raw glazes. Thermophysical modeling is able to calculate the liquidus temperature of a raw glaze as a function of its composition and oxygen activity during firing. Glazes that are fired to temperatures higher than their liquidus temperatures are more likely to be transparent or have shiny surfaces, while firing temperatures lower than their liquidus temperature are more likely to result in matt or opaque surfaces.

Iron glazes fired under oxidizing and reducing atmospheres can have very different colors and surface finishes. This is due to changes in the iron oxidation state. For glazes containing a high iron fraction, the primary phase field shift from hematite to magnetite accompanied by a decrease in the liquidus temperature. An increase in the fraction of FeO, a silicate network modifier, lowers its viscosity of the molten phase.

The precipitation of thermodynamically stable high temperature phases actively removes secondary fluxes from the melt. The secondary fluxes transition from being anti-fluxing to fluxing between 60 to 130 °C below the liquidus temperature.

Silicate liquid immiscibility is predicted for a sizable number of the raw glaze recipes considered in this study, which may result in the formation of a low-viscosity Ca-rich molten phase and a high viscosity Ca-poor molten phases. On average, the two-phase viscosity values are is 22% lower on average compared with their corresponding single-phase viscosity values. Correctly identifying the continuous phase in an immiscible silicate melt is a significant

challenge in viscosity modeling, particularly when the two molten phases are similar in their volume fraction.

Experimental measurements of raw glaze viscosity factors are in agreement with a multiple linear regression model based on the liquidus temperature and peak firing temperature viscosity as calculated with two viscosity models. This may be helpful in identifying promising candidates for glaze recipes or evaluating new raw glaze minerals.

Lead glazes have peak firing temperature viscosity values that are significantly lower than lead-free glazes. The peak firing temperature viscosity of the latter is consistent with the working point of glass. Boil up (i.e., formation of closed or burst bubbles) can be avoided by limiting glaze viscosity to less than 40 Pa·s or higher than 600 to 900 Pa·s, as proposed by Nosova [4] in a study of fritted glazes. Molten lead glazes are expected to have effective viscosities lower than 40 Pa·s, while lead-free glazes have effective viscosities greater than the 600 to 900 Pa·s range.

Thermophysical modeling provides a unifying framework for understanding molten raw glaze viscosity under disparate firing conditions. The approach allows for rapid evaluation of changes in raw glaze viscosity as a function of composition, temperature, and oxygen activity. The approach is also helpful in furthering an understanding of changes in the composition of molten and solid phases present during the firing of raw glazes, particularly in the absence of experimentally measured quantities.

Acknowledgements

This research did not receive any specific grant from funding agencies in the public, commercial, or not-for-profit sectors.

References

[1] E. Cooper, The Potter's Book of Glaze Recipes, 2nd ed., University of Pennsylvania Press, Philadelphia, 2004.

[2] B. Burzacchini, M. Paganelli, H.G. Christ, Examination of Fast-Fire Frits and Glazes Using a Hot Stage Microscope at Different Heating Rates, in: A Collection of Papers Presented at the 97th Annual Meeting and the 1995 Fall Meetings of the Materials & Equipment/Whitewares: Ceramic Engineering and Science Proceedings, 1996, pp. 60-66.

[3] M. Ahmed, D.A. Earl, Characterizing glaze-melting behavior via HSM, Am Ceram Soc Bull, 81 (2003) 47-51.

[4] Z.A. Nosova, Influence of physical properties of glaze on the quality of a glazed surface, Glass Ceram+, 14 (1957) 164-170.

[5] E. Bou, A. Moreno, A. Escardino, A. Gozalbo, Microstructural study of opaque glazes obtained from frits of the system: SiO_2-Al_2O_3-B_2O_3-(P_2O_5)-CaO-K_2O-TiO_2, J Eur Ceram Soc, 27 (2007) 1791-1796.

[6] S. Salem, S.H. Jazayeri, F. Bondioli, A. Allahverdi, M. Shirvani, Characterizing thermal behavior of ceramic glaze containing nano-sized cobalt-aluminate pigment by hot stage microscopy, Thermochim Acta, 521 (2011) 191-196.

[7] F.M. Stábile, M. Piccico, M.F. Serra, M. Rafti, G. Súarez, N.M. Rendtorff, Viscosity and thermal evolution of density and wetting angle of a commercial glaze by means of hot stage microscopy, Proc Mat Sci, 9 (2015) 563-570.

[8] A. Tunali, E. Ozel, S. Turan, Production and characterisation of granulated frit to achieve anorthite based glass-ceramic glaze, J Eur Ceram Soc, 35 (2015) 1089-1095.

[9] J.K. Beam, Effect of opacifiers on fused viscosity of feldspathic glazes, J Am Ceram Soc, 26 (1943) 205-212.

[10] H. Scholze, Der Einfluss von Viskosität und Oberflächenspannung auf erhitzungsmikroskopische Messungen an Gläsern, Ber Dtsch Keram Ges, 39 (1962) 63–68.

[11] L. Fröberg, T. Kronberg, L. Hupa, M. Hupa, Influence of firing parameters on phase composition of raw glazes, J Eur Ceram Soc, 27 (2007) 1671-1675.

[12] T. Kronberg, L. Hupa, Melting behaviour of raw glazes, J Eur Ceram Soc, 39 (2019) 4404-4416.

[13] P.J. Spencer, A brief history of CALPHAD, Calphad, 32 (2008) 1-8.

[14] S.A. Decterov, A.N. Grundy, I.H. Jung, A.D. Pelton, Modeling the viscosity of aluminosilicate melts, in: T.E. Simos, G. Maroulis (Eds.) Computation in Modern Science and Engineering, AIP, Corfu, Greece, 2007, pp. 404-407.

[15] P.Y. Hsieh, Effects of temperature non-uniformity and effective viscosity on pyrometric cone deformation, Int J Ceram Eng Sci, 1 (2019) 216-226.

[16] P.Y. Hsieh, Viscous deformation as a measure of heat work during coal ash fusibility testing, Fuel, 281 (2020) 118723.

[17] A.R. McBirney, T. Murase, Rheological properties of magmas, Annu Rev Earth Pl Sc, 12 (1984) 337-357.

[18] H.F. Staley, L.C. Hewitt, The cost of raw lead glazes, T Am Ceram Soc, 19 (1917) 657-673.

[19] C.F. Binns, The Potter's Craft: A Practical Guide for the Studio and Workshop, D. Van Nostrand Company, New York, 1922.

[20] F.H. Rhead, Painting in underglaze colors on the biscuit, J Am Ceram Soc, 5 (1922) 376-384.

[21] J.W. Dougherty, Pottery Made Easy, Bruce Publishing Company, Milwaukee, 1955.

[22] W. Heimsoeth, F.R. Meyer, Viscosity studies of titania porcelain enamels, J Am Ceram Soc, 34 (1951) 366-370.

[23] M.J. Pascual, A. Durán, M.O. Prado, A new method for determining fixed viscosity points of glasses, Phys Chem Glasses, 46 (2005) 512-520.

[24] A.V. Astin, Standard Reference Material 711: Lead-Silica Glass, in, National Bureau of Standards, Gaithersburg, MD, 1964.

[25] W.P. Reed, Standard Reference Material 710a: Soda-Lime-Silica Glass, in, National Institute of Standards and Technology, Gaithersburg, MD, 1991.

[26] H. Ishibashi, Non-Newtonian behavior of plagioclase-bearing basaltic magma: subliquidus viscosity measurement of the 1707 basalt of Fuji volcano, Japan, J Volcanol Geoth Res, 181 (2009) 78-88.

[27] M.O. Chevrel, C. Cimarelli, L. deBiasi, J.B. Hanson, Y. Lavallée, F. Arzilli, D.B. Dingwell, Viscosity measurements of crystallizing andesite from Tungurahua volcano (Ecuador), Geochem Geophy Geosy, 16 (2015) 870-889.

[28] E. Roedder, Silicate liquid immiscibility in magmas and in the system K_2O-FeO-Al_2O_3-SiO_2: an example of serendipity, Geochim Cosmochim Ac, 42 (1978) 1597-1617.

[29] R. Pal, Novel viscosity equations for emulsions of two immiscible liquids, J Rheol, 45 (2001) 509-520.

[30] R. Sarkar, Refractory Technology: Fundamentals and Applications, CRC Press, Boca Raton, FL, 2016.

[31] M. Tribaudino, R.J. Angel, F. Cámara, F. Nestola, D. Pasqual, I. Margiolaki, Thermal expansion of plagioclase feldspars, Contrib Mineral Petr, 160 (2010) 899–908

[32] R. Knoche, D.B. Dingwell, S.L. Webb, Melt densities for leucogranites and granitic pegmatites: partial molar volumes for SiO_2, Al_2O_3, Na_2O, K_2O, Li_2O, Rb_2O, Cs_2O, MgO, CaO, SrO, BaO, B_2O_3, P_2O_5, F_2O_{-1}, TiO_2, Nb_2O_5, Ta_2O_5, and WO_3, Geochim Cosmochim Ac, 59 (1995) 4645-4652.

[33] S. Fujino, C. Hwang, K. Morinaga, Density, surface tension, and viscosity of PbO-B_2O_3-SiO_2 glass melts, J Am Ceram Soc, 87 (2004) 10-16.

[34] Q. Liu, R.A. Lange, The partial molar volume of Fe_2O_3 in alkali silicate melts: evidence for an average Fe^{3+} coordination number near five, Am Mineral, 91 (2006) 385-393.

[35] J. Lee, L.T. Hoai, J. Choe, J.H. Park, Density measurements of CaO-MnO-SiO_2 slags, ISIJ Int, 52 (2012) 2145-2148.

[36] X. Guo, R.A. Lange, Y. Ai, Density and sound speed measurements on model basalt (An–Di–Hd) liquids at one bar: new constraints on the partial molar volume and compressibility of the FeO component, Earth Planet Sc Lett, 388 (2014) 283-292.

[37] H.P. Zhang, H.A. Makse, Jamming transition in emulsions and granular materials, Phys Rev E, 72 (2005).

[38] A. Ikeda, L. Berthier, P. Sollich, Unified study of glass and jamming rheology in soft particle systems, Phys Rev Lett, 109 (2012).

[39] S. Mueller, E.W. Llewellin, H.M. Mader, The rheology of suspensions of solid particles, P Roy Soc A-Math Phy, 466 (2010) 1201-1228.

[40] M. Bailey, Glazes Cone 6: 1240°C/2264°F, University of Pennyslvania Press, Philadelphia, 2001.

[41] H. Ries, W.S. Bayley, High-grade clays of the eastern United States with notes on some western clays, in, U.S. Geological Survey, Washington, DC, 1922.

[42] P. Rogers, Phil Rogers: An Autobiography, in: Ceramics Monthly, American Ceramic Society, Westerville, OH, 1993, pp. 31-36.

[43] C.W. Davis, H.C. Vacher, Bentonite: its properties, mining, preparation, and utilization, in, Bureau of Mines, Washington, DC, 1928.

[44] H. Van Olphen, J.J. Fripiat, Data Handbook for Clay Materials and Other Non-Metallic Minerals, in, Pergamon Press, New York, 1979, pp. xiv, 346 p.

[45] M. Ostermann, The New Maiolica: Contemporary Approaches to Colour and Technique, Craftsman House, North Ryde, N.S.W., 1999.

[46] J.H. Weis, J.E. Boyd Jr, Carolina stone, J Am Ceram Soc, 20 (1937) 62-63.

[47] M. Obstler, Ceramic Raw Materials, in, Ceramic Publications Company, 2010.

[48] A. Orío, J. Corella, I. Narváez, Characterization and Activity of Different Dolomites for Hot Gas Cleaning in Biomass Gasification, in: A.V. Bridgwater, D.G.B. Boocock (Eds.) Developments in Thermochemical Biomass Conversion: Volume 1 / Volume 2, Springer Netherlands, Dordrecht, 1997, pp. 1144-1157.

[49] C.L. Babcock, Preparation of Laboratory Glass Samples, in: K. Lark-Horovitz, V.A. Johnson (Eds.) Solid State Physics, Academic Press, New York, 1959.

[50] F.W. Clarke, Analyses of rocks and minerals from the laboratory of the United States Geological Survey, 1880 to 1914, in, U.S. Geological Survey, Washington, D.C., 1915.

[51] Industrial Mineral Products, "True Albany" Slip Clay, in, Albany, NY, 1985.

[52] J.E. Kogel, N.C. Trivedi, J.M. Barker, S.T. Krukowski, Industrial Minerals & Rocks: Commodities, Markets, and Uses, Society for Mining, Metallurgy, and Exploration, Littleton, CO, 2006.

[53] F. Hamer, J. Hamer, The Potter's Dictionary of Materials and Techniques, 5th ed., University of Pennsylvania Press, Philadelphia, 2004.

[54] Vanderbilt Minerals, VANSIL® Wollastonite, in, Norwalk, CT, 2016.

[55] I.J. McColm, Dictionary of Ceramic Science and Engineering, Springer Verlag, 2016.

[56] F.E. Fowle, Smithsonian Physical Tables, in, Smithsonian Institution, Washington, 1920.

[57] J.H. Hodgkinson, F.D. Stacey, Practical Handbook of Earth Science, CRC Press, Boca Raton, FL, 2017.

[58] F.W. Clarke, The data of geochemistry, in, U.S. Geological Survey, Washington, DC, 1920.

[59] W.M. Haynes, CRC Handbook of Chemistry and Physics, in, CRC Press, Boca Raton, FL, 2014.

[60] D.R. Lide, CRC Handbook of Chemistry and Physics, 73rd ed., CRC Press, Boca Raton, FL, 1993.

[61] M. Ocaña, A. Caballero, T. González-Carreño, C.J. Serna, Preparation by pyrolysis of aerosols and structural characterization of Fe-doped mullite powders, Mater Res Bull, 35 (2000) 775-788.

[62] W. Schumann, Minerals of the World, 2nd ed., Sterling, New York, 2008.

[63] J.A. Miller, Titanium: a materials survey, in, Bureau of Mines, Washington, DC, 1957.

[64] D.L. Perry, Handbook of Inorganic Compounds, 2nd ed., CRC Press, Boca Raton, 2016.

[65] A. Fluegel, Glass viscosity calculation based on a global statistical modelling approach, Glass Technology-European Journal of Glass Science and Technology Part A, 48 (2007) 13-30.

[66] D. Giordano, J.K. Russell, D.B. Dingwell, Viscosity of magmatic liquids: a model, Earth Planet Sc Lett, 271 (2008) 123-134.